

US stock market interaction network as learned by the Boltzmann Machine

Stanislav S. Borysov,^{1,2,*} Yasser Roudi,^{1,3} and Alexander V. Balatsky^{1,4}

¹*Nordita, KTH Royal Institute of Technology and Stockholm University,
Roslagstullsbacken 23, SE-106 91 Stockholm, Sweden*

²*Nanostructure Physics, KTH Royal Institute of Technology,
Roslagstullsbacken 21, SE-106 91 Stockholm, Sweden*

³*The Kavli Institute for Systems Neuroscience, NTNU, 7030 Trondheim*

⁴*Institute for Materials Science, Los Alamos National Laboratory, Los Alamos, NM 87545, USA*

(Dated: June 28, 2022)

We study historical dynamics of joint equilibrium distribution of stock returns in the US stock market using the Boltzmann distribution model being parametrized by external fields and pairwise couplings. Within Boltzmann learning framework for statistical inference, we analyze historical behavior of the parameters inferred using exact and approximate learning algorithms. Since the model and inference methods require use of binary variables, effect of this mapping of continuous returns to the discrete domain is studied. Properties of distributions of external fields and couplings as well as industry sector clustering structure are studied for different historical dates and moving window sizes. We show that discrepancies between them might be used as a precursor of financial instabilities.

PACS numbers: 89.65.Gh, 02.50.Tt, 64.70.kj

I. INTRODUCTION

Price formation on a financial market is a complex problem: It reflects opinion of investors about true value of the asset in question, policies of the producers, external regulation and many other factors. Given the big number of factors influencing price, many of which unknown to us, describing price formation essentially requires probabilistic approaches. In the last decades, synergy of methods from various scientific areas has opened new horizons in understanding the mechanisms that underlie related problems. One of the popular approaches is to consider a financial market as a complex system, where not only a great number of constituents plays crucial role but also non-trivial interaction properties between them [1, 2]. For example, related interdisciplinary studies of complex financial systems have revealed their enhanced sensitivity to fluctuations and external factors near critical events [3–6] with overall change of internal structure [7, 8]. This can be complemented by the research devoted to equilibrium [9–12] and non-equilibrium [13, 14] phase transitions.

In general, statistical modeling of the state space of a complex system requires writing down the probability distribution over this space using real data. In a simple version of modeling, the probability of an observable configuration (state of a system) described by a vector of variables \mathbf{s} can be given in the exponential form

$$p(\mathbf{s}) = \mathcal{Z}^{-1} \exp \{-\beta \mathcal{H}(\mathbf{s})\}, \quad (1)$$

where \mathcal{H} is the Hamiltonian of a system, β is inverse temperature (further $\beta \equiv 1$ is assumed) and \mathcal{Z} is a statis-

tical sum. Physical meaning of the model's components depends on the context and, for instance, in the case of financial systems, \mathbf{s} can represent a vector of stock returns and \mathcal{H} can be interpreted as the inverse utility function [15]. Generally, \mathcal{H} has parameters defined by its series expansion in \mathbf{s} . Basing on the maximum entropy principle [16, 17], expansion up to the quadratic terms is usually used, leading to the pairwise interaction models. In the equilibrium case, the Hamiltonian has form

$$\mathcal{H}(\mathbf{s}) = -\mathbf{h}^\top \mathbf{s} - \mathbf{s}^\top \mathbf{J} \mathbf{s}, \quad (2)$$

where \mathbf{h} is a vector of size N of external fields and \mathbf{J} is a symmetric $N \times N$ matrix of couplings (\top denotes transpose). The model may also involve hidden states (nodes), which are not directly observable, but here we restrict ourselves to considering the visible nodes case only.

The energy-based models represented by Eq. (1) play essential role not only in statistical physics but also in neuroscience (models of neural networks [18, 19]) and machine learning (generative models, also known as Boltzmann machines [20]). Recently, applications of the pairwise interaction models to financial markets have been also explored [15, 21–23]. Given topological similarities between neural and financial networks [24], these systems can be considered as examples of complex adaptive systems [25], which are characterized by the adaptation ability to changing environment, trying to stay in equilibrium with it. From this point of view, market structural properties, e.g. clustering and networks [26–28], play important role for modeling of the distribution of stock prices. Adaptation (or learning) in these systems implies change of the parameters of \mathcal{H} as financial and economic systems evolve. Using statistical inference for the model's parameters, the main goal is to have a model capable of reproducing the same statistical observables

* stanislav@smart.mit.edu; Present address: Singapore-MIT Alliance for Research and Technology, 1 CREATE Way, #09-02, Create Tower, 138602 Singapore

given time series for a particular historical period. In the pairwise case, the objective is to have

$$\begin{aligned} \langle s_i \rangle_{\text{data}} &= \langle s_i \rangle_{\text{model}}, \\ \langle s_i s_j \rangle_{\text{data}} &= \langle s_i s_j \rangle_{\text{model}}, \end{aligned} \quad (3)$$

where angular brackets denote statistical averaging over time.

Having specified general mathematical model, one can also discuss similarities between financial and infinite-range magnetic systems in terms of phenomena related, e.g. extensivity, order parameters and phase transitions, etc. These features can be captured even in the simplified case, when s_i is a binary variable taking only two discrete values. Effect of the mapping to a binarized system, when the values $s_i = +1$ and $s_i = -1$ correspond to profit and loss respectively, is also studied in the paper. In this case, diagonal elements of the coupling matrix, J_{ii} , are zero because $s_i^2 = 1$ terms do not contribute to the Hamiltonian. It is worth stressing that the current investigation develops ideas outlined in the previous studies [15, 21–23] in a way that the effect of binarization, comparison of learning algorithms, evolution and scaling properties of the parameters distributions are studied in a more systematic fashion.

The paper is organized as follows. In Section II, basic statistical definitions and inference methods for \mathbf{h} and \mathbf{J} are presented. In the Section III, effect of binarization of stock returns and historical evolution of the model parameters are discussed. Finally, the main findings of our investigation are summarized in Section IV.

II. DATA AND METHODS

We study historical dynamics of the US stock market using $N = 71$ stock prices time series [29] from the Standard & Poor's 500 index (hereafter S&P 500) listed in Table I. We analyze discrete daily closing prices, $S_i(t)$, starting from 1990 till 2013 (5828 trading days), which are converted to logarithmic returns, $s_i^{\text{raw}}(t) = \ln[S_i(t)/S_i(t-1)]$.

A. Basic statistical analysis of financial time series

The top panel in Fig. 1(a) shows historical data for the average stock return. In order to extract long-term trends from the time series, we employ a simple moving window (or simple moving average, SMA) approach. It acts like a low-pass filter, filtering out high frequency components, which are usually related to noise. Within the SMA approach, data is divided into chunks (or windows) of size T , assuming the time series to be stationary on this scale. In this case, t th chunk corresponds to T equally weighted previous values of daily log-returns (including the current one). For each set of chunks, one can calculate different statistical characteristics, such as

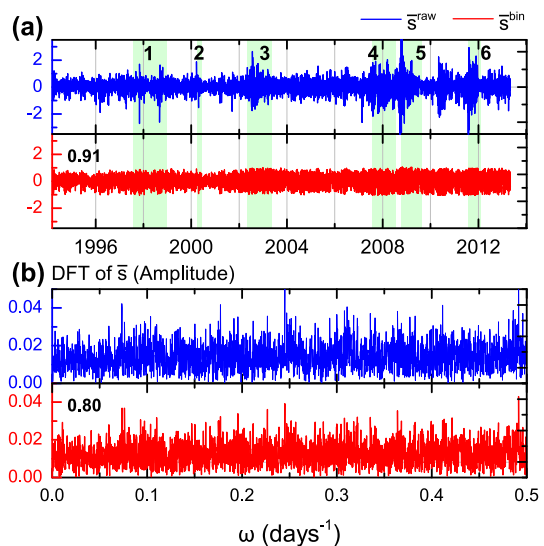


FIG. 1. Historical dynamics of the mean raw and binary return (a) and amplitudes of their Discrete Fourier transforms (b). The distance between two labeled dates is 1000 trading days. A few major financial crises are highlighted with a light green background: (1) Asian and Russian crisis of 1997–1998, (2) dot-com bubble, (3) US stock market downturn of 2002, (4) US housing bubble, (5) bankruptcy of Lehman Brothers followed by the global financial crisis, (6) European sovereign debt crisis. Numbers in panels show correlation between the corresponding series. Historical values of average return, economic cycles and frequency of crashes are preserved for the binary returns despite the maximum magnitude being bounded.

average

$$\langle s_i \rangle = \frac{1}{T} \sum_{t'=0}^{T-1} s_i(t'), \quad (4)$$

and *covariance matrix*, \mathbf{C} ($N \times N$), with the elements

$$C_{ij} = \langle s_i s_j \rangle - \langle s_i \rangle \langle s_j \rangle, \quad (5)$$

where $T \geq N$ assumed for the covariance matrix to be positive definite. Hereinafter, angular brackets $\langle \rangle$ denote averaging over time (historical values), while bar $\bar{}$ denotes averaging over index (vector or matrix elements). It is also possible to investigate nonlinear dependence between time series using more sophisticated statistical concepts [30] or nonlinear data transformations, however only the simplest linear case is considered in the current paper. Series *variance* is autocovariance, $\sigma_i^2 \equiv C_{ii}$, where σ denotes *standard deviation* or *volatility* in finance. Usually, SMA volatility serves as the simplest risk measure quantifying stability of returns. In order to quantify deviation from the normal distribution, it is also useful to define higher-order moments, such as *skewness*

$$\langle \text{Skew}(s_i) \rangle = \left\langle \left(\frac{s_i - \langle s_i \rangle}{\sigma_i} \right)^3 \right\rangle \quad (6)$$

and *kurtosis* (also known as excess kurtosis)

$$\langle \text{Kurt}(s_i) \rangle = \frac{\langle (s_i - \langle s_i \rangle)^4 \rangle}{\sigma_i^4} - 3, \quad (7)$$

which equal zero in the Gaussian case. Indeed, SMA filter allows one to extract long-term trends in the market and, for a large value of N , various moments of returns distribution can be used to identify market crashes (Figs. 2 and 3). Henceforth, we will call the considered portfolio “market” as it represents a big number of the top companies from S&P500 index.

As mentioned in the Introduction, to reduce the amount of data required for our inference, we focus on a binarized version of the returns and not on the raw data. We thus define the binarized version of the returns as

$$s_i^{\text{bin}} = \text{sign}(s_i^{\text{raw}}). \quad (8)$$

This procedure also mitigates the scaling problem of multiple series since it assigns the same value of stock return independently of its absolute value. Another common technique to deal with this problem is standardization

$$s_i^{\text{std}} = \frac{s_i^{\text{raw}} - \langle s_i^{\text{raw}} \rangle}{\sigma_i}. \quad (9)$$

In this case, *correlation matrix*, \mathbf{Q} ($N \times N$), is a normalized covariance matrix with the elements

$$Q_{ij} = \frac{C_{ij}}{\sigma_i \sigma_j}. \quad (10)$$

Standardization procedure is known to preserve market behavior and widely used for the statistical analysis of the financial time series [31]. Effects of these mappings defined by Eqs. (8)–(10) are shown in Figs. 1–3 and will be discussed further in Section III where we will compare some simple statistical properties of the binarized return versus the raw and standardized returns. Before this, however, we briefly describe the inference procedure.

B. Equilibrium Boltzmann learning methods

We harness inference methods based on maximizing of the model’s likelihood $\mathcal{L}(\mathbf{h}, \mathbf{J} \mid \mathbf{s}^{\text{data}})$. In the equilibrium case, exact learning of the Hamiltonian [Eq. (2)] parameters implies solving Eq. (3) in a self-consistent way, where corrections δh_i and δJ_{ij} on each learning step can be calculated as

$$\begin{aligned} \delta h_i &= \eta_h (\langle s_i \rangle_{\text{data}} - \langle s_i \rangle_{\text{model}}), \\ \delta J_{ij} &= \eta_J (\langle s_i s_j \rangle_{\text{data}} - \langle s_i s_j \rangle_{\text{model}}). \end{aligned} \quad (11)$$

Here, η_h and η_J are learning rates, $\langle \cdot \rangle_{\text{data}}$ are empirical (observed) moments and $\langle \cdot \rangle_{\text{model}}$ are the moments sampled from the model using Monte Carlo (MC) methods.

The exact learning algorithm always yields optimal values for \mathbf{h} and \mathbf{J} if there are no hidden nodes in the system [32].

Being in general slow, the exact learning algorithm might be substituted by the approximate inference methods [33] which are based on expansion of the free energy of a system for small fluctuations around its mean value. The first-order (naïve) approximation within the mean field theory (nMF) gives

$$\begin{aligned} \mathbf{J}^{\text{nMF}} &= \mathbf{A}^{-1} - \mathbf{C}^{-1}, \\ h_i^{\text{nMF}} &= \tanh^{-1} \langle s_i \rangle - \sum_{j=1}^N J_{ij}^{\text{nMF}} \langle s_j \rangle, \end{aligned} \quad (12)$$

where $A_{ij} = (1 - \langle s_i \rangle^2) \delta_{ij}$ and δ_{ij} is the Kronecker delta. Here, taking into account the diagonal element J_{ii} (which is usually discarded) for the calculation of corresponding h_i improves accuracy of the approximation, being known as the diagonal-weight trick [33]. The second-order correction to nMF requires solving Thouless-Anderson-Palmer equations (TAP)

$$\begin{aligned} (\mathbf{C}^{-1})_{ij} &= -J_{ij}^{\text{TAP}} - 2 (J_{ij}^{\text{TAP}})^2 \langle s_i \rangle \langle s_j \rangle, \\ h_i^{\text{TAP}} &= h_i^{\text{nMF}} - \langle s_i \rangle \sum_{j=1}^N (J_{ij}^{\text{TAP}})^2 (1 - \langle s_i \rangle^2), \end{aligned} \quad (13)$$

where Eq. (12) should be used instead for the calculation of the external fields if the diagonal-weight trick is used.

III. RESULTS AND DISCUSSION

A. Effect of binarization

The mapping defined by Eq. (8) obviously affects information contained in the time series. In order to estimate this effect, we compare time series for the average raw and binary returns first. As Fig. 1 shows, correlation coefficient between historical values of \bar{s}^{raw} and \bar{s}^{bin} is very high (0.91). Moreover, correlation between amplitudes of their Fourier transforms is also high (0.80), suggesting that signatures of economic cycles and frequency of market crashes are preserved in the binarized time series. However, maximum magnitude of binary returns is obviously bounded by the definition.

Comparison of the filtered time series using SMA also indicates preserving information about market trends in the binarized time series. With this aim, we compare historical evolution of the first four moments of the distribution of average binarized versus raw and standardized returns. Using SMA window $T = 250$ trading days (approximately one trading year), the results presented in Fig. 2(a) indicate that the binary returns behave similar to raw and standardized returns, preserving dynamics of the first two moments and less so about the third moment, while information about kurtosis is lost for all T [Fig. 2(b)]. Regarding the pairwise correlations, Figure 3(a) shows that the covariance matrix of binarized

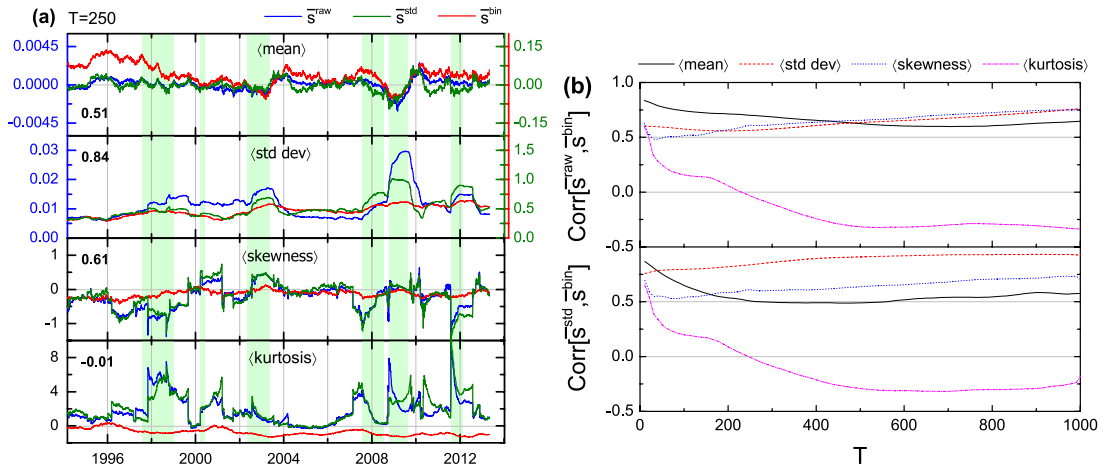


FIG. 2. Historical dynamics of the first four moments of the distribution of the mean market return (a). Top-bottom: temporal mean, standard deviation, skewness and kurtosis calculated using SMA window of 250 days for the raw (blue) and binary (red) returns of 71 US stocks (Table I). A number in each panel corresponds to overall historical correlation between the time series for standardized and binarized returns. Dependence of these overall correlations on the moving window size is shown in (b). Binary returns behave similar to raw and standardized returns, however information about kurtosis is completely lost.

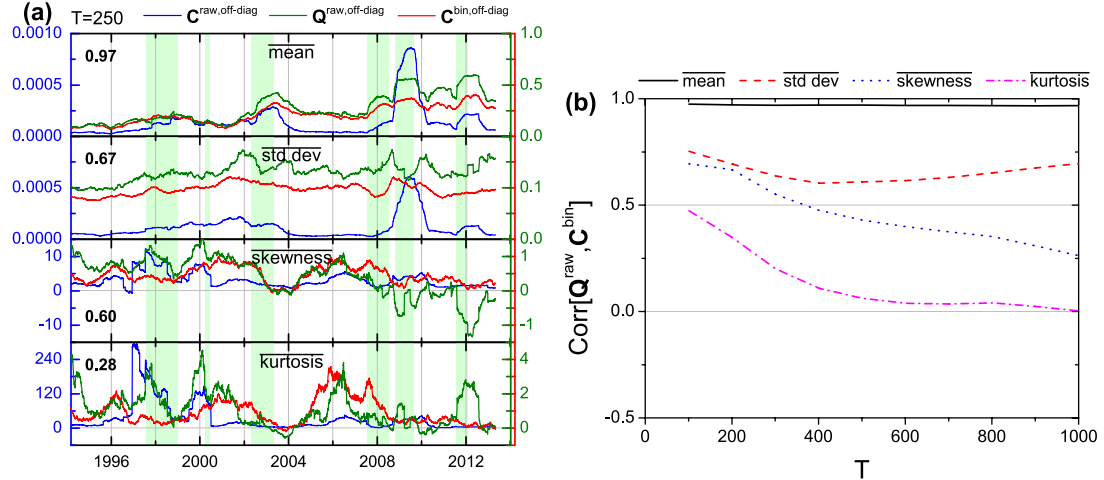


FIG. 3. Historical dynamics of the first four moments of the distribution of the off-diagonal elements of covariance (blue) and correlation (green) matrices of raw returns, and covariance matrix of binary returns (red) calculated using SMA window of 250 days (a). Top-bottom: mean, standard deviation, skewness and kurtosis of the off-diagonal elements of the matrices. A number in each panel corresponds to overall historical correlation between the time series for standardized and binarized returns. Dependence of these overall correlations on the moving window size is shown in (b). Binarization makes covariance matrix similar to the correlation matrix of raw returns.

returns becomes similar to the correlation matrix of raw returns. Indeed, off-diagonal elements follow similar distributions with very high correlation between means. For higher-order moments, correlation decreases with T [Fig. 3(b)].

Having validated that binary returns capture market historical behavior similarly to standardized returns, we proceed to the Boltzmann model inference and evolution of its parameters.

B. Comparison of approximate and exact learning methods

Following SMA approach with $T = 250$ trading days, we study historical evolution of the external fields and couplings inferred for each chunk of the binarized time series. We use two approximate (nMF and TAP) learning methods and compare them with exact learning, where MC sampling is used for the latter.

Figure 4 shows comparison of the inferred parameters for four different historical dates. Without use of the diagonal-weight trick, inference of external fields in the

nMF case works better when the dates far from market crashes are considered (top row in the two leftmost columns, corresponding to 22 Dec 1997 and 09 Jan 2002). TAP correction slightly improves the inference accuracy however producing overestimated values in comparison with the exact learning algorithm (second row). Both approximations perform worse for the data near market crashes (two top rows in the two rightmost columns, corresponding to 09 Oct 2008 and 13 March 2012). While the diagonal-weight trick allows to achieve almost perfect accuracy in both cases (red triangles in the first two rows), justifying the need of high-order corrections. Couplings inferred using both approximations show the same trend, being more/less accurate far from/near crashes (bottom row). Although the bulk of couplings is in an agreement with the exact couplings even near crashes, positive outliers are overestimated. Historical dynamics of the inference quality is depicted in Fig. 5, where normalized root mean square error

$$\text{NRMSE}(\mathbf{x}, \mathbf{y}) = \sqrt{\frac{\overline{(x_i - y_i)^2}}{\overline{(y_i - \bar{y})^2}}} \quad (14)$$

and correlation between the model parameters inferred using different methods are presented. It confirms that the diagonal-weight trick considerably improves inference quality of the external fields and the couplings are systematically overestimated.

To validate the results obtained by the exact learning algorithm, we sampled stock returns from the model using MC sampling. The single and pairwise empirical moments are nicely recovered from the exact model (figures are not shown), while the third-order covariances, $\langle (s_i - \langle s_i \rangle)(s_j - \langle s_j \rangle)(s_k - \langle s_k \rangle) \rangle$, are almost not captured by the model (Fig. 6). Although this could be due to the lack of data for estimating the real third-order covariances, this is unlikely to be the case as the degree of mismatch between the third-order covariances of the Ising model and the data is the same even when the bigger amount of data is used for their estimation. Nevertheless, in spite of the fact that individual third-order covariances are not captured well, historical dynamics of their mean can be recovered from the model (Fig. 7).

C. Distribution of inferred parameters

Figure 8 shows histograms of the external fields and couplings inferred using the exact learning algorithm for three different window sizes: $T = 250, 1000$ and 5000 trading days. Distribution of the external fields is close to the Gaussian and does not possess outliers independently of T . Bulk of the couplings is also distributed normally, however a positive heavy tail is present. For bigger window sizes, the Gaussian bulk component of the inferred couplings becomes less prominent and the tail starts to dominate. In fact, as shown in Fig. 9, all moments of the distribution of J_{ij} scale with T . On the contrary, there

is no obvious dependence for h_i , which behavior is close to the external fields inferred from randomly shuffled time series (where each element is swapped with other randomly picked element using uniform distribution within the moving window chunk). Higher value of \bar{h} inferred on randomly shuffled time series can be explained by the fact that it compensates positive (ferromagnetic) contribution to the mean return stemming from the positive mean of the inferred couplings: In the shuffled case, \bar{J} becomes zero while all $\langle s_i^{\text{bin}} \rangle$ remain unaffected, therefore this effect should be compensated by the external fields.

Historical dynamics of the moments of the distributions shown in Fig. 10 indicates that the average external field is strongly correlated with the mean return (0.90), while higher moments seem not to convey any particular information about market historical behavior. Without use of the diagonal-weight trick, \bar{h}^{nMF} is completely inconsistent with \bar{h}^{Exact} [Fig. 10(a)]. Although h_i^{TAP} behave more similar to h_i^{Exact} , they are significantly overestimated. At the same time, the diagonal-weight trick allows to achieve almost perfect accuracy in both cases [Fig. 10(b)]. Distribution of couplings has stable small positive mean corresponding to ferromagnetic interaction, however with almost half of couplings being negative, i.e. the system is likely to exhibit frustrated configurations.

It is also interesting to note that the standard deviation of couplings far from crashes almost linearly increases over the whole period considered from 0.14 in 1996 to 0.2 in 2013 [the second panel in Fig. 10(c)]. This observation gains more meaning when we note that the standard deviation of the couplings in 1996 equals approximately to the standard deviation of the couplings inferred on randomly shuffled returns, while its value is almost twice bigger than one for the shuffled time series in 2013. Also, during the biggest market crashes, standard deviation of couplings has jumps because interconnections on the market become tighter as a result of the herding behavior during a financial turmoil: Until system is not adapted to a new economic reality, prices tend to move collectively with overall market performance as a benchmark [34]. The positive heavy tail, which can be characterized by higher order moments, increases for some historical periods. A reason for it is unknown at the moment.

D. Industry-related clustering structure

It is well known that a stock market possesses a hierarchical clustering structure which can be detected using correlations [26, 35] or couplings [15, 23] between stocks. One of the most popular techniques employed to find related structures is based on the minimum spanning tree (MST) algorithm. For instance, Prim's algorithm—a basic MST construction algorithm—consists of the three following steps:

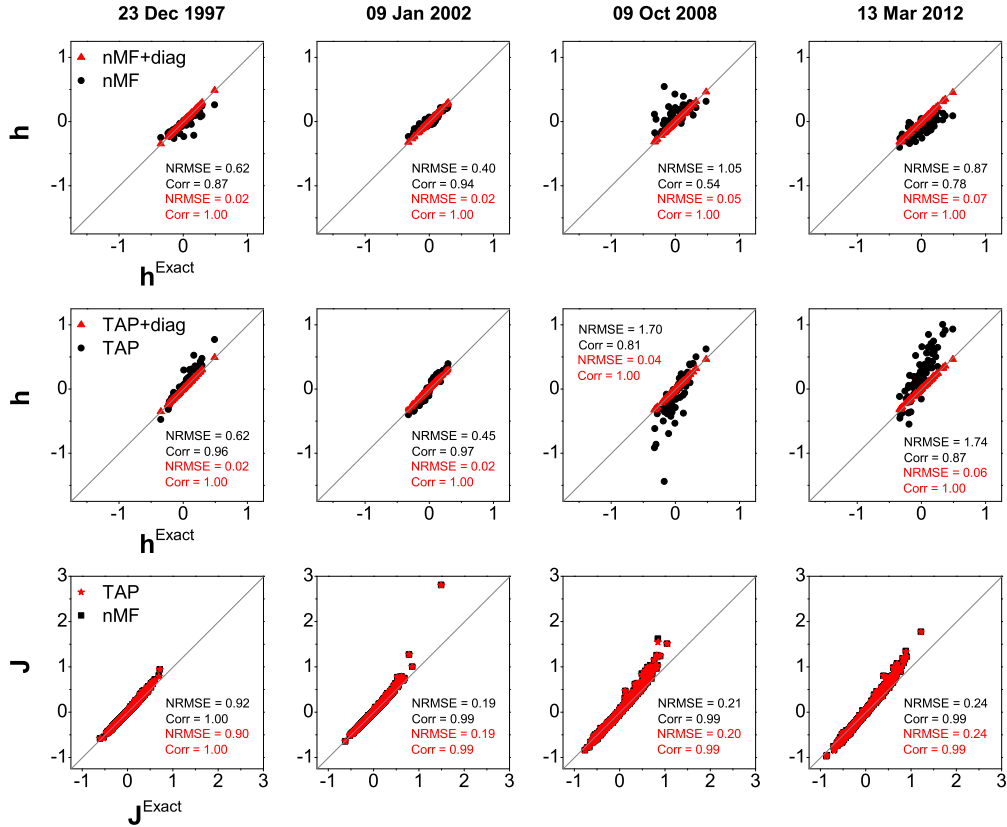


FIG. 4. Comparison of external fields (two top rows) and couplings (bottom row) inferred using the exact and approximate (nMF and TAP) learning algorithms for four different historical dates and SMA window of 250 trading days. The diagonal-weight trick is essential for correct inference of external fields. Both approximate learning algorithms overestimate couplings with big absolute values.

1. Initialize a tree with a single stock, chosen arbitrarily from the all stocks.
2. Find the stock not yet in the tree which has the strongest coupling (biggest value of C_{ij} or J_{ij}) to a stock in the tree and include it to the tree.
3. Repeat step 2 until all stocks are in the tree.

Figure 11 shows examples of the MST constructed using covariance and coupling matrices of binary stock returns. The remarkable feature of these structures is a manifestation of industry sector clustering. Here, we define an industry sector cluster as a connected subset of the tree where all stocks belong to the same industry sector, i.e. each cluster member interacts to the other members only through the stocks from the same sector. Further, we denote cluster size as $N_{m,k}$, where $m = 1 \dots M$ is a sector index ($M = 9$ is the total number of sectors listed in Table I) and $k = 1 \dots K_m$ is an index of the cluster (K_m is a number of such clusters for the sector m).

As mentioned above, there can be many clusters for each industry sector. In order to estimate overall industry clustering degree of the market, let us introduce a simple metric based on finding clusters of the maximum

size

$$Q_{\text{mst}} = \frac{1}{N} \sum_{m=1}^M \max_k N_{m,k}. \quad (15)$$

Intuitively, when Q_{mst} is small it reflects the fact that stocks do not tend to group basing on industry sectors. Its minimum value corresponding to M/N is defined by the situation where the biggest cluster for each sector has only one stock, i.e. K_m equals to the total number of stocks in the sector m . The maximum value of Q_{mst} is 1, which corresponds to the perfect industry clustering structure when there is only one cluster for each industry sector ($K_m = 1$). This clustering measure shows interesting dependence on the size of moving window (Fig. 12), suggesting an increasing degree of sectoral connectedness of the stock market for bigger time windows as inferred by the Ising model. Also, the degree of connectedness increases with the increase of non-Gaussian features (skewness and kurtosis) of couplings distribution.

To further investigate network structure and clustering degree of \mathbf{J} , we perform the clustering analysis based on a subset of J_{ij} . With this aim, we choose a threshold, J^{th} , and construct MST only using $J_{ij} < J^{\text{th}}$. Figure 13 suggests that neither the biggest nor negative val-

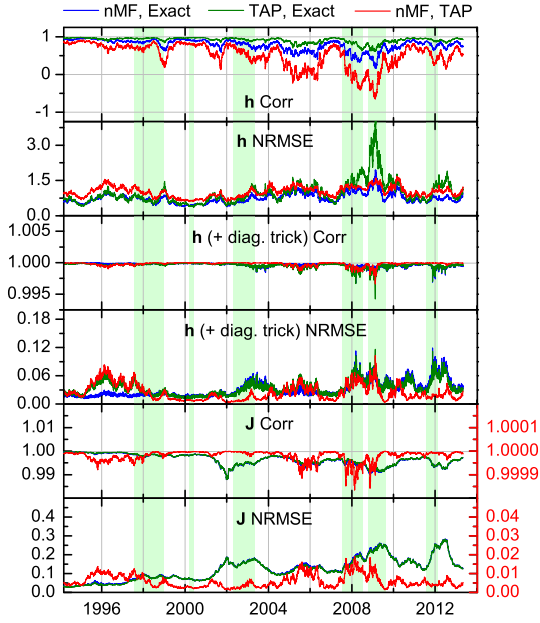


FIG. 5. Comparison (normalized root mean square error and correlation coefficient) of the external fields and couplings inferred using different methods: nMF versus exact (blue), TAP versus exact (green) and nMF versus TAP (red). Without the use of the diagonal-weight trick, approximation quality of the external fields is very low and significantly drops during financial crashes (two top panels), while making use of the trick improves it considerably (two middle panels). Couplings inferred using both approximate methods are almost the same, with approximation quality being lower during the periods of financial crises (two bottom panels).

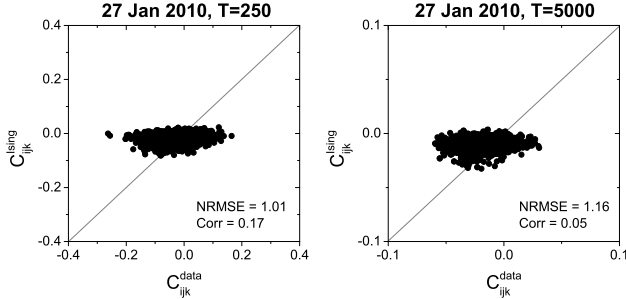


FIG. 6. Comparison of the third-order covariances calculated using the real data and 50000 MC samples from the exact Ising model for two different moving window sizes. The Ising model is not capable of recovering observed individual third-order covariances independently of moving window size.

ues of J_{ij} seem not to contain information about the observed industry-related clustering structure: The biggest increase of Q_{mst} occurs only when J^{th} is bigger than zero, while it is almost insensitive to the inclusion of J_{ij} from a heavy tail. Finally, it is also worth noting that intraday internal structure of couplings is neither stable (quenched) nor completely random (annealed), preserving an industry-related clustering structure with the

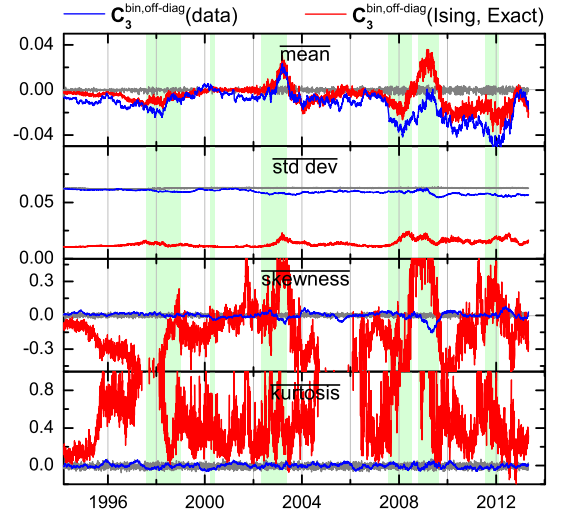


FIG. 7. Historical evolution of the first four moments of distribution of the third-order covariances calculated using real (blue), randomly shuffled (gray) and 5000 MC samples (for each historical date) from the exact Ising model (red) data. The exact Ising model is only capable of capturing historical dynamics of the mean value of the empirical third-order covariances. However, all higher moments for the real data behave similarly to the ones calculated on randomly shuffled time series.

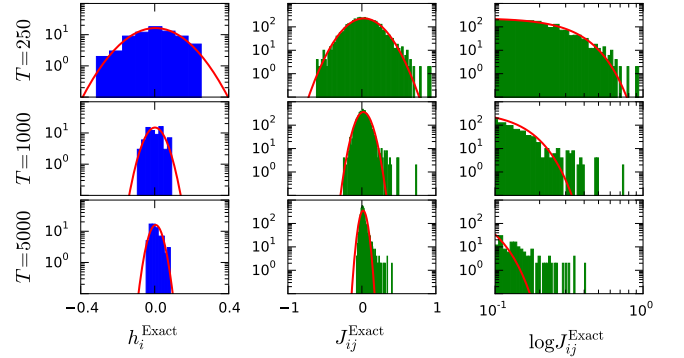


FIG. 8. Histograms of the external fields and couplings inferred using the exact learning algorithm for 27 Jan 2010 for three different moving window sizes. Red curve denotes Gaussian fit. For small moving window sizes, the bulk of couplings is distributed normally, while a positive heavy tail dominates for bigger sizes of moving window.

diameter being smaller during crashes (figures are not shown). These non-trivial features of a coupling matrix will be studied in more detail in the future works.

E. Scaling of inferred parameters

In order to study extensive properties of the system, we investigate scaling properties of the parameter distributions with the number of stocks, which are usually

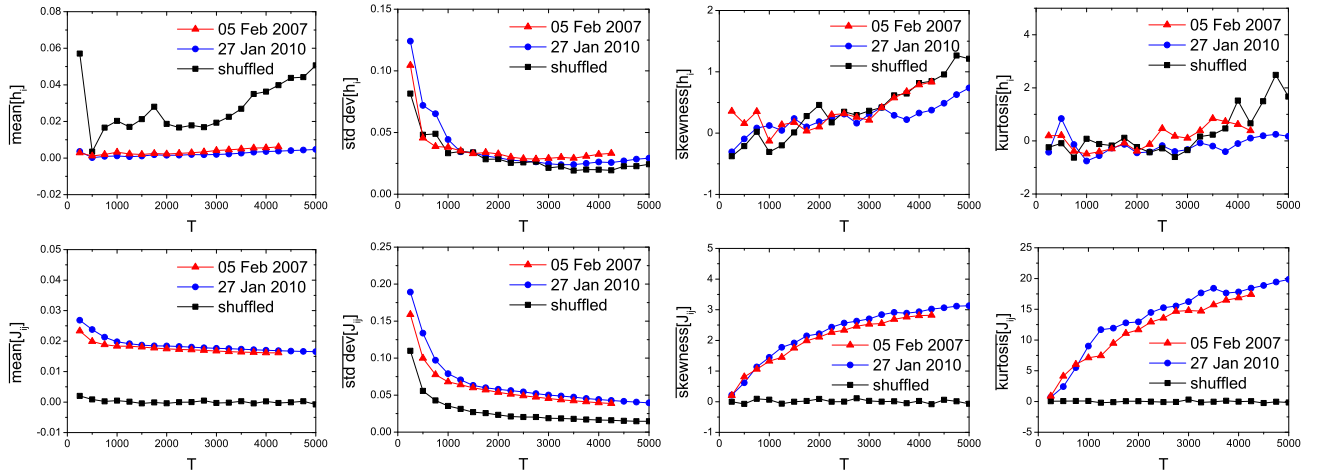


FIG. 9. Scaling of the first four moments of exact external fields distribution (top row) and couplings (bottom row) with moving window size T for two different historical dates and randomly shuffled time series for 27 Jan 2010. Higher value of the mean value of the external fields inferred on randomly shuffled time series compensates positive (ferromagnetic) contribution to the mean return of the mean value of couplings, which is zero for the shuffled time series.

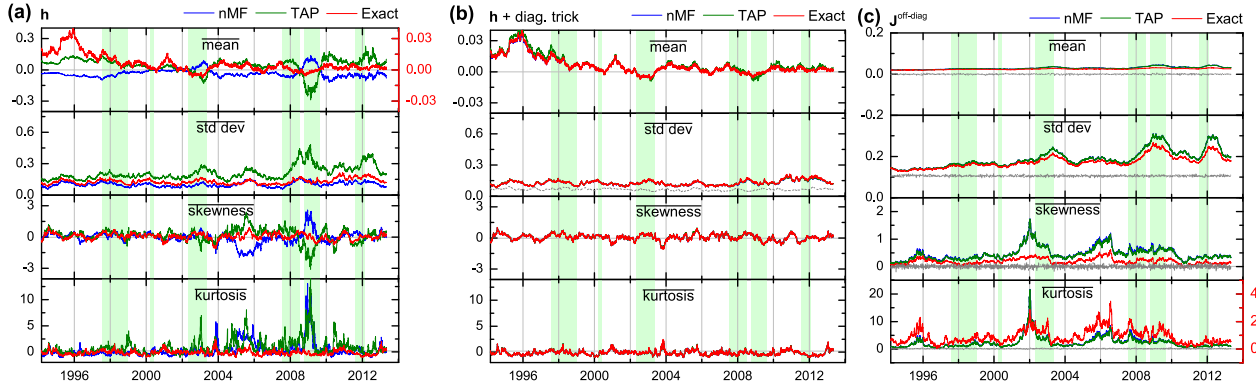


FIG. 10. Historical dynamics of the first four moments of distribution of the external fields inferred without (a) and with (b) use of the diagonal-weight trick, off-diagonal couplings (c) inferred using naive mean field (blue), TAP (green) and exact (red) inference algorithms. Both mean field approximations incorrectly estimate external fields without use of the diagonal-weight trick and tend to overestimate couplings. During periods of crisis, increase of couplings strength is observed because of stronger correlations on the market. Moments of the couplings and external fields distributions inferred on randomly shuffled returns are denoted with the gray dashed line.

characterized by the scaling exponent N^α . We estimate its value for each distribution moment as the average over scaling exponents for randomly selected subsets of stocks of different size.

As Fig. 14 (top row) shows, external fields distribution does not possess any particular scaling law, except the mean, which has α close to -0.75 . The other moments scale similar to the corresponding moments of the external fields inferred on randomly shuffled time series. Scaling properties of couplings distribution depends on the size of moving window (Fig. 14, bottom row). When T is small, couplings behave similar to the ones inferred on randomly shuffled returns. However, scaling of the mean and standard deviation becomes closer to the properties of the normal distribution with growth of T . This dependence might be related to the presence of finite-size

effects, when use of a small number of historical values is not enough to estimate true correlations on the market.

There are two extreme ways in which a change in the distribution of the couplings can arise as one increases the size of the observed system. One is that the structure between the previous stocks entirely changes by adding new stocks. Alternatively, the couplings could only change their absolute magnitude, while they maintain their magnitude relative to one another. To better understand where in this spectrum our financial market exists, we performed analysis similar to Ref. [19]: We chose a random subset of 20 stocks and analyzed couplings between them for different total number of stocks taken into account for the inference (including the original 20). Figure 15 shows that the biggest/smallest values of J_{ij} remain the same with growth of N and their scal-

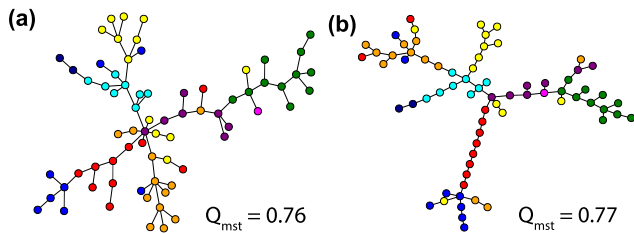


FIG. 11. Minimum spanning tree for the covariance matrix (a) and corresponding exact couplings (b) for 27 Jan 2010 calculated using SMA window $T = 4000$ trading days. Similar industry-related clustering structure is observed in both cases. The considered sectors are Healthcare (red), Consumer Goods (blue), Basic Materials (green), Financial (cyan), Industrial Goods (purple), Services (yellow), Technology (orange), Conglomerate (magenta) and Utilities (dark blue). The graphs are visualized using the NetworkX Python package [36].

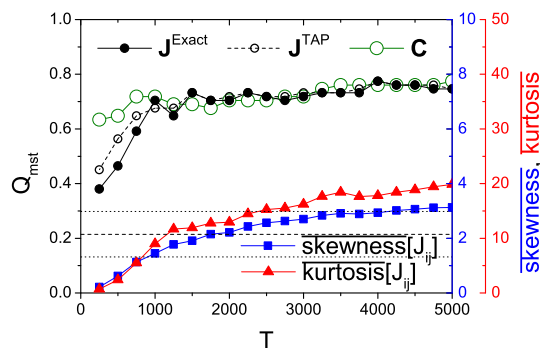


FIG. 12. Quality (industry sector clustering degree) of minimum spanning tree, Q_{mst} , depending on moving window size for exact and TAP couplings, and covariance matrix (27 Jan 2010). Gray dashed and dotted lines denote mean and 99.7% confidence interval respectively for the quality of MST built on randomly shuffled time series. Quality of MST for couplings increases with deviation of their distribution from the Gaussian, which is characterized by skewness and kurtosis.

ing becomes closer to the normal distribution for bigger time windows. This behavior also suggests that important features of market connectivity are preserved with the number of stocks.

F. External and internal influence

Considering the two terms in the system's Hamiltonian [Eq. (2)], it is also possible to define internal and external influences in the market. For this purpose, external fields can be interpreted as the influence of external factors, $\mathbf{h}^{\text{ext}} \equiv \mathbf{h}$, while couplings define internal bias, $\mathbf{h}^{\text{int}} = \langle \mathbf{s}^T \rangle \mathbf{J}$ (in the MF sense) [22]. In this case, external contribution corresponds to the individual stocks biases which come from outside the market, while internal one is solely defined in terms of internal market interactions. Similarly, one can also define two energy terms as

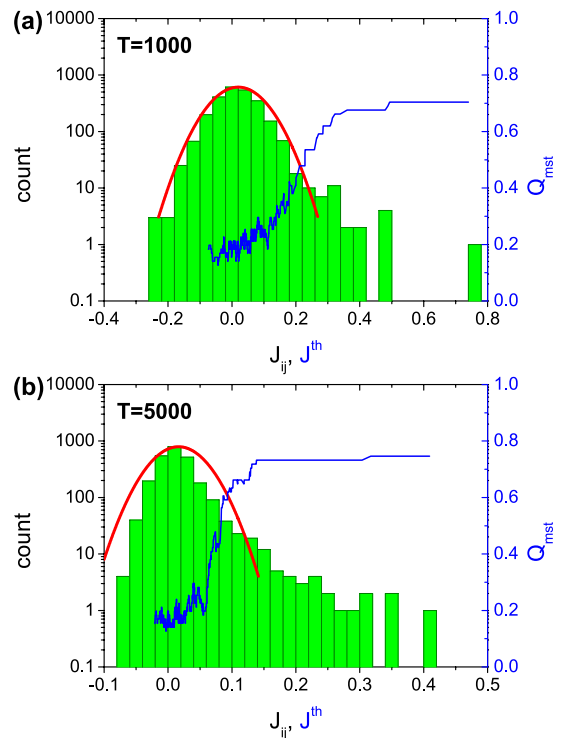


FIG. 13. Exact couplings distribution (27 Jan 2010) for two SMA windows $T = 1000$ (a) and $T = 5000$ (b) trading days, and quality (industry sector clustering degree) of minimum spanning tree, Q_{mst} , (blue solid line) depending on the positive cutoff, J^{th} , of the couplings used for MST construction. Red curve denotes Gaussian fit. Discarding the biggest couplings does affect quality of MST unless the cutoff is not close to the bulk of the distribution. Negative couplings do not contribute to the market clustering structure.

$\mathcal{H} = E^{\text{ext}} + E^{\text{int}}$, where $E^{\text{ext,int}} = -(\mathbf{h}^{\text{ext,int}})^T \langle \mathbf{s} \rangle$. Figure 16 shows that both energies have almost the same order of magnitude over the historical period considered, while near the major crashes E^{ext} is more than 10 times bigger than E^{int} . The ratio between the mean biases also possesses interesting historical dynamics. Being in principle strongly correlated with the mean return (0.9 for \bar{h}^{ext} and 0.99 for \bar{h}^{int}), discrepancies between them might be used as a leading indicator of financial instabilities. Away from the periods of crisis, the ratio is almost stable, while divergent behavior is observed before the US market crashes (two bottom panels in Fig. 16). Possible explanation of the observed behavior from a financial point of view is still an open question.

IV. CONCLUSION

We have investigated various aspects of application of the pairwise interaction model to financial time series. The model, being parametrized by external fields and couplings, is used for the approximation of the joint equilibrium distribution of stock returns. Since the consid-

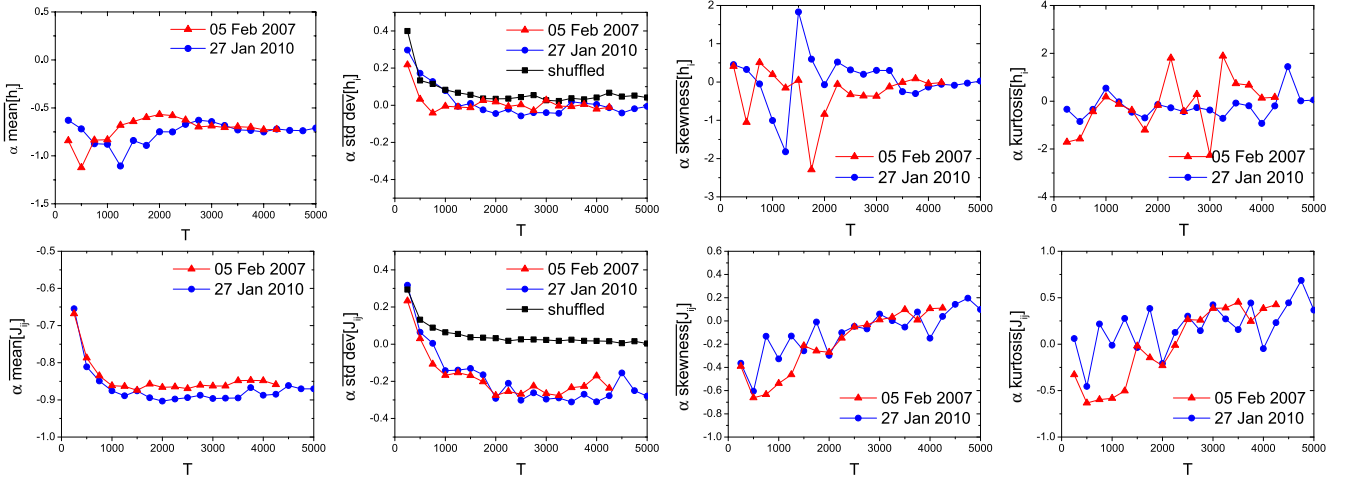


FIG. 14. Average scaling exponent with number of stocks, α , for the exact external fields (top row) and couplings (bottom row) distributions depending on moving window size, T , for two different historical dates and randomly shuffled time series for 27 Jan 2010. Scaling exponent of the mean of external fields is close to -0.75 for big values of T , while the higher moments scale similar to the external fields inferred on randomly shuffled time series. Empirical couplings behave similar to the couplings inferred on randomly shuffled time series for small window sizes, while their scaling properties become closer to the properties of the Gaussian distribution for bigger values of T .

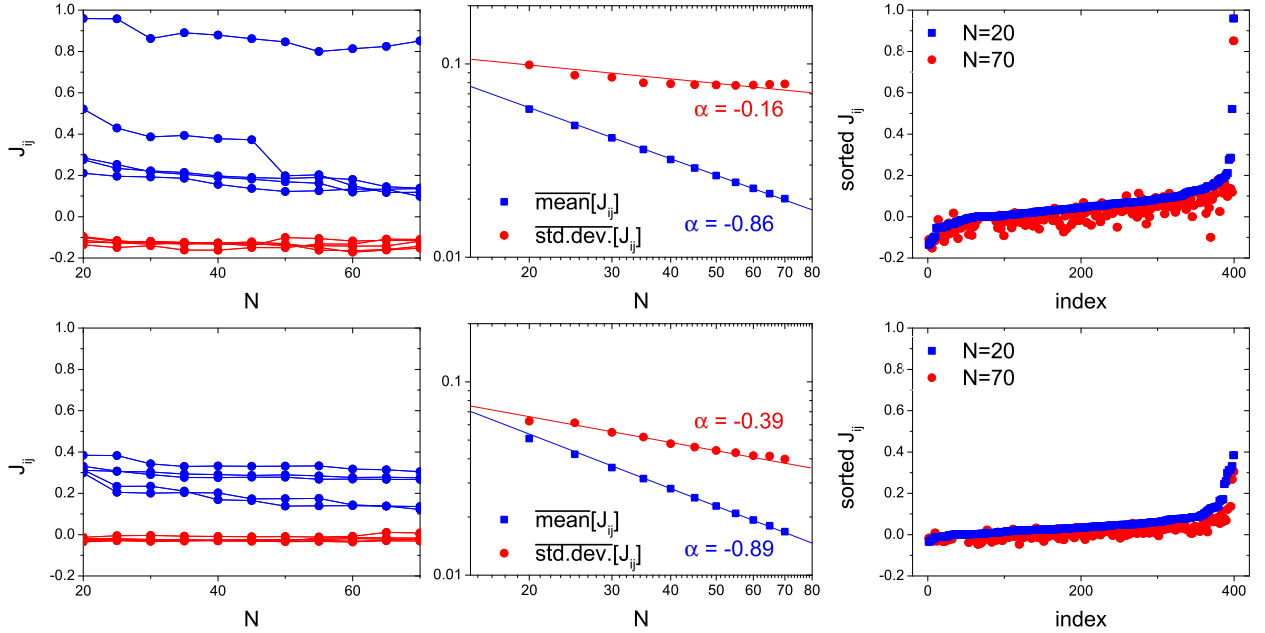


FIG. 15. Scaling of the 380 couplings between a randomly selected subset of 20 stocks depending on total number of stocks used for the inference (including original 20) for 27 Jan 2010 and $T = 1000$ (top row) and $T = 5000$ (bottom row): 10 biggest/smallest couplings (first column), mean and standard deviation of the couplings (second column) and their visualization (third column). Relative magnitude of the couplings decreases as the number of stocks grows, while the underlying network structure is preserved.

ered learning algorithms require use of binary variables, the logarithmic returns are binarized using the sign function. Effect of the binarization suggests that the distribution of binary returns captures the distributions of raw and standardized returns to a good degree, preserving information about economic cycles and market crashes as well as industry-related market clustering structure.

The model parameters are inferred using approximate and exact learning algorithms. Mean field approximations nicely recover bulk of the couplings except outliers. External fields are in the almost perfect agreement with the exact algorithm if the diagonal-weight trick is used. The obtained results also suggest that the quality of mean field inference methods drops in the periods of

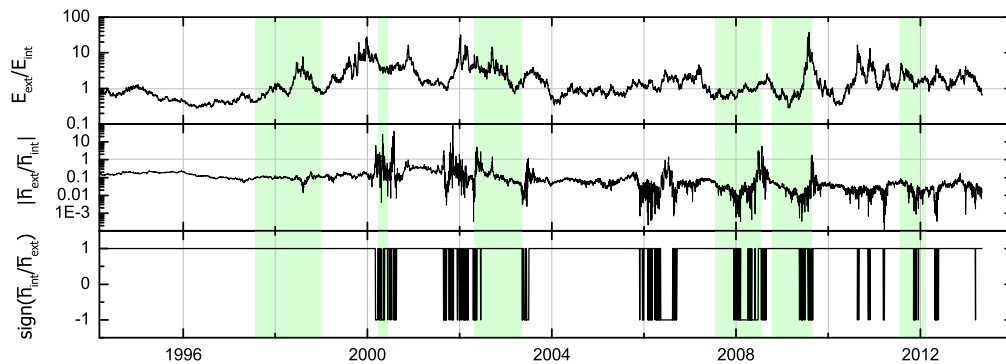


FIG. 16. Comparison of external and internal biases for the exact Ising model. Top-bottom: ratio of external and internal energies contributing to the Hamiltonian, absolute value of the ratio of the mean external and internal biases and its sign. Major market crashes are preceded by growth of the external energy and discrepancy between the biases.

financial crises due to increase of magnitude of the parameters. This behavior observed near market crashes can be viewed as an adaptation process, when a financial market structure evolves to equilibrate with a new economic reality.

For the historical period considered, distribution of external fields is close to the Gaussian and does not possess any outliers independently of moving window size. On the contrary, distribution of couplings possesses a heavy positive tail, which starts to dominate over the Gaussian bulk for bigger moving window sizes. Mean of external fields decreases with the number of stocks while their standard deviation remains almost constant, corresponding to the standard deviation of the external fields inferred on randomly shuffled time series. Scaling properties of the couplings distribution depends on the moving window size, becoming closer to the properties of the Gaussian distribution with its growth.

Despite possible presence of finite-size effects, an industry-related clustering structure is observed for both

exact and approximate couplings. The performed cut-off analysis suggests that neither the biggest positive nor negative values of couplings do not contain information about this structure. Scaling properties of the couplings between a small random subset of stocks suggest that the underlying network structure is also preserved with the number of stocks. These non-trivial structural properties of a coupling matrix as well as their historical dynamics will be studied in the future works.

Finally, the pairwise interaction model also allows one for defining the external and internal biases which correspond to contribution of external fields and couplings respectively. Discrepancies between them might be used as a precursor of imminent financial instabilities and should be studied more deeply from a financial point of view.

V. ACKNOWLEDGMENTS

This work is supported by Nordita, VR VCB 621-2012-2983, the Marie Curie Training Network NETADIS (FP7, grant 290038), the Kavli Foundation and the Norwegian Research Councils Centre of Excellent Scheme.

-
- [1] N. F. Johnson, P. Jefferies, and P. M. Hui, *Financial Market Complexity* (Oxford University Press, Oxford, 2003).
 - [2] D. Sornette, *Why Stock Markets Crash: Critical Events in Complex Financial Systems* (Princeton University Press, Princeton, NJ, 2009).
 - [3] R. Albert and A.-L. Barabási, *Rev. Mod. Phys.* **74**, 47 (2002).
 - [4] K. Kacperski and J. A. Hołyst, *Phys. Lett. A* **254**, 53 (1999).
 - [5] K. Kiyono, Z. R. Struzik, and Y. Yamamoto, *Phys. Rev. Lett.* **96**, 068701 (2006).
 - [6] A.-L. Barabási and R. Albert, *Science* **286**, 509 (1999).
 - [7] S. N. Dorogovtsev and J. F. F. Mendes, *Evolution of Networks: From Biological Nets to the Internet and WWW (Physics)* (Oxford University Press, New York, NY, 2003).
 - [8] S. Bornholdt and H. G. Schuster, eds., *Handbook of Graphs and Networks: From the Genome to the Internet* (John Wiley & Sons, New York, NY, 2003).
 - [9] P. Gai and S. Kapadia, *Philos. Trans. R. Soc. Lond. A* **466**, 2401 (2010).
 - [10] M. Newman, *SIAM Rev. Soc. Ind. Appl. Math.* **45**, 167 (2003).
 - [11] P. Fronczak, A. Fronczak, and J. A. Hołyst, *Eur. Phys. J. B* **59**, 133 (2007).
 - [12] S. H. Strogatz, *Nature* **410**, 268 (2001).
 - [13] P. Holme and M. E. J. Newman, *Phys. Rev. E* **74**, 056108 (2006).
 - [14] K. Klemm, V. M. Eguíluz, R. Toral, and M. San Miguel, *Phys. Rev. E* **67**, 026120 (2003).
 - [15] T. Bury, *Physica A* **392**, 1375 (2013).
 - [16] E. T. Jaynes, *Phys. Rev.* **106**, 620 (1957).
 - [17] E. T. Jaynes, *Phys. Rev.* **108**, 171 (1957).

- [18] E. Schneidman, M. J. Berry, R. Segev, and W. Bialek, *Nature* **440**, 1007 (2006).
- [19] Y. Roudi, J. Tyrcha, and J. Hertz, *Phys. Rev. E* **79**, 051915 (2009).
- [20] Y. LeCun, S. Chopra, R. Hadsell, M. Ranzato, and F. J. Huang, in *Predicting Structured Data* (The MIT Press, Cambridge, MA, 2007) pp. 191–246.
- [21] J. Maskawa, *Physica A* **311**, 563 (2002).
- [22] T. Bury, *Eur. Phys. J. B* **86**, 1 (2013).
- [23] H.-L. Zeng, R. Lemoy, and M. Alava, *J. Stat. Mech.* **2014**, P07008 (2014).
- [24] P. E. Vértes, R. M. Nicol, S. Chapman, N. Watkins, D. A. Robertson, and E. T. Bullmore, *Front. Syst. Neurosci.* **5**, 75 (2011).
- [25] C. Hommes, *Quant. Financ.* **1**, 149 (2001).
- [26] R. Mantegna, *Eur. Phys. J. B* **11**, 193 (1999).
- [27] J.-P. Onnela, A. Chakraborti, K. Kaski, J. Kertsz, and A. Kanto, *Phys. Scr.* **2003**, 48 (2003).
- [28] G. Bonanno, G. Caldarelli, F. Lillo, S. Miccichè, N. Vandewalle, and R. Mantegna, *Eur. Phys. J. B* **38**, 363 (2004).
- [29] <http://www.finance.yahoo.com/>.
- [30] C. Lee, J. Lee, and A. Lee, *Statistics for Business and Financial Economics*, 3rd ed. (Springer, New York, NY, 2013).
- [31] D. J. Fenn, M. A. Porter, S. Williams, M. McDonald, N. F. Johnson, and N. S. Jones, *Phys. Rev. E* **84**, 026109 (2011).
- [32] S.-I. Amari, K. Kurata, and H. Nagaoka, *IEEE Trans. Neural. Netw.* **3**, 260 (1992).
- [33] T. Tanaka, *Phys. Rev. E* **58**, 2302 (1998).
- [34] S. S. Borysov and A. V. Balatsky, *PLoS ONE* **9**, e105874 (2014).
- [35] R. Coelho, S. Hutzler, P. Repetowicz, and P. Richmond, *Physica A* **373**, 615 (2007).
- [36] A. A. Hagberg, D. A. Schult, and P. J. Swart, in *Proceedings of the 7th Python in Science Conference (SciPy2008)* (Pasadena, CA USA, 2008) pp. 11–15.

TABLE I. List of the companies which stock prices are used for the calculations in the paper.

Ticker	Name	Sector	Ticker	Name	Sector
ABT	Abbott Laboratories	Hea	AIG	American International Group, Inc.	Fin
AMGN	Amgen Inc.	Hea	APA	Apache Corp.	Bas
APC	Anadarko Petroleum Corp.	Bas	AAPL	Apple Inc.	Con
AXP	American Express Company	Fin	BA	The Boeing Company	Ind
BAC	Bank of America Corp.	Fin	BAX	Baxter International Inc.	Hea
BMJ	Bristol-Myers Squibb Company	Hea	C	Citigroup, Inc.	Fin
CAT	Caterpillar Inc.	Ind	CELG	Celgene Corporation	Hea
CL	Colgate-Palmolive Co.	Con	CMCSA	Comcast Corporation	Ser
COP	ConocoPhillips	Bas	COST	Costco Wholesale Corp.	Ser
CSCO	Cisco Systems, Inc.	Tec	CVS	CVS Caremark Corp.	Ser
CVX	Chevron Corp.	Bas	DD	E. I. du Pont de Nemours and Co.	Bas
DE	Deere & Company	Ind	DELL	Dell Inc.	Tec
DHR	Danaher Corp.	Ind	DIS	The Walt Disney Company	Ser
DOW	The Dow Chemical Company	Bas	EMC	EMC Corporation	Tec
EMR	Emerson Electric Co.	Tec	EOG	EOG Resources, Inc.	Bas
EXC	Exelon Corp.	Uti	F	Ford Motor Co.	Con
GE	General Electric Company	Ind	HAL	Halliburton Company	Bas
HD	The Home Depot, Inc.	Ser	HON	Honeywell International Inc.	Ind
HPQ	Hewlett-Packard Company	Tec	IBM	International Business Machines Corp.	Tec
INTC	Intel Corp.	Tec	JNJ	Johnson & Johnson	Hea
JPM	JPMorgan Chase & Co.	Fin	KO	The Coca-Cola Company	Con
LLY	Eli Lilly and Company	Hea	LOW	Lowe's Companies Inc.	Ser
MCD	McDonald's Corp.	Ser	MDT	Medtronic, Inc.	Hea
MMM	3M Company	Cng	MO	Altria Group Inc.	Con
MRK	Merck & Co. Inc.	Hea	MSFT	Microsoft Corp.	Tec
NKE	Nike, Inc.	Con	ORCL	Oracle Corporation	Tec
OXY	Occidental Petroleum Corp.	Bas	PEP	Pepsico, Inc.	Con
PFE	Pfizer Inc.	Hea	PG	The Procter & Gamble Company	Con
PNC	The PNC Financial Services Group	Fin	SLB	Schlumberger Limited	Bas
SO	Southern Company	Uti	T	AT&T, Inc.	Tec
TGT	Target Corp.	Ser	TJX	The TJX Companies, Inc.	Ser
TXN	Texas Instruments Inc.	Tec	UNH	UnitedHealth Group Incorporated	Hea
UNP	Union Pacific Corp.	Ser	USB	U.S. Bancorp	Fin
UTX	United Technologies Corp.	Ind	VZ	Verizon Communications Inc.	Tec
WFC	Wells Fargo & Company	Fin	WMT	Wal-Mart Stores Inc.	Ser
XOM	Exxon Mobil Corp.	Bas			

Industry sectors are defined as Basic Materials (Bas), Conglomerate (Cng), Consumer Goods (Con), Financial (Fin), Healthcare (Hea), Industrial Goods (Ind), Services (Ser), Technology (Tec) and Utilities (Uti).